EBioMedicine 40 (2019) 675–684

Contents lists available at ScienceDirect

EBioMedicine

journal homepage: www.ebiomedicine.com

EBioMedicine
Published by THE LANCET

Primary cardiac manifestation of autosomal dominant polycystic kidney disease revealed by patient induced pluripotent stem cell-derived cardiomyocytes

Jia-Jung Lee [a,b,c,d], Sin-Jhong Cheng [e,f], Ching-Ying Huang [e], Chen-Yun Chen [e], Li Feng [g,h], Daw-Yang Hwang [b,c], Timothy J. Kamp [g,i,j], Hung-Chun Chen [b,c,d,**], Patrick C.H. Hsieh [e,g,j,*]

[a] Ph.D. Program in Translational Medicine, Kaohsiung Medical University and Academia Sinica, Taiwan
[b] Division of Nephrology, Department of Internal Medicine, Kaohsiung Medical University Hospital, Kaohsiung, Taiwan
[c] Faculty of Medicine, College of Medicine, Kaohsiung Medical University, Kaohsiung, Taiwan
[d] Faculty of Renal Care, College of Medicine, Kaohsiung Medical University, Kaohsiung, Taiwan
[e] Institute of Biomedical Sciences, Academia Sinica, Taipei, Taiwan
[f] Neuroscience Program of Academia Sinica, Academia Sinica, Taipei, Taiwan
[g] Cellular and Molecular Arrhythmia Research Program, University of Wisconsin-Madison, Madison, WI, United States
[h] Department of Cardiology, Beijing AnZhen Hospital, Capital Medical University, Beijing, China
[i] Department of Cell and Regenerative Biology, University of Wisconsin-Madison, Madison, WI, United States
[j] Department of Medicine, University of Wisconsin-Madison, Madison, WI, United States

ARTICLE INFO

Article history:
Received 30 October 2018
Received in revised form 28 December 2018
Accepted 7 January 2019
Available online 11 January 2019

Keywords:
Human iPS cell
Autosomal dominant polycystic kidney disease
Cardiomyocyte
Arrhythmia

ABSTRACT

Background: Mutations in *PKD1* or *PKD2* gene lead to autosomal dominant polycystic kidney disease (ADPKD). The mechanism of ADPKD progression and its link to increased cardiovascular mortality is still elusive.
Methods: We differentiated ADPKD patient induced pluripotent stem cells (iPSCs) to cardiomyocytes (CMs). The electrophysiological properties at the cellular level were analyzed by calcium imaging and whole cell patch clamping.
Findings: The ADPKD patient iPSC-CMs had decreased sarcoplasmic reticulum calcium content compared with Control-CMs. Spontaneous action potential of the *PKD2* mutation line-derived CMs demonstrated slower beating rate and longer action potential duration. The *PKD1* mutation line-derived CMs showed a comparable dose-dependent shortening of phase II repolarization with the Control-CMs, but a significant increase in beating frequency in response to L-type calcium channel blocker. The *PKD1*-mutant iPSC-CMs also showed a relatively unstable baseline as a greater percentage of cells exhibited delayed afterdepolarizations (DADs). Both the ADPKD patient iPSC-CMs showed more β-adrenergic agonist-elicited DADs compared with Control-CMs.
Interpretation: Characterization of ADPKD patient iPSC-CMs provides new insights into the increased clinical risk of arrhythmias, and the results enable disease modeling and drug screening for cardiac manifestations of ADPKD.
Fund: Ministry of Science and Technology, National Health Research Institutes, Academia Sinica Program for Technology Supporting Platform Axis Scheme, Thematic Research Program and Summit Research Program, and Kaohsiung Medical University Hospital, Taiwan.

1. Introduction

Autosomal dominant polycystic kidney disease (ADPKD) is the most common monogenic kidney disorder with an estimated prevalence of 1:400–1:1000 [1]. Besides pathognomonic bilateral renal cysts and familial kidney failure, ADPKD has extra-renal manifestations and is considered a systemic disease [1,2]. Cardiovascular complications are the major cause of ADPKD patient mortality [3,4]. To date, we still lack effective treatment for ADPKD [5,6]. Patients with ADPKD have increased incidence of early onset hypertension, left ventricular hypertrophy,

* Correspondence to: P. C.H. Hsieh, Institute of Biomedical Sciences, Academia Sinica, 128 Academia Road, Section 2, Nankang, Taipei 11529, Taiwan.
** Correspondence to: H. C. Chen, Division of Nephrology, Kaohsiung Medical University Hospital; Faculty of Medicine, Faculty of Renal Care, College of Medicine, Kaohsiung Medical University, 100 Shih-Chuan 1st Road, Kaohsiung 80708, Taiwan.
E-mail addresses: chenhc@kmu.edu.tw (H.-C. Chen), phsieh@ibms.sinica.edu.tw (P.C.H. Hsieh).

https://doi.org/10.1016/j.ebiom.2019.01.011

Research in context

Evidence before this study

Human iPSCs from ADPKD patients or human iPSCs with mutated-*PKD* gene have been used in research as iPSC-derived epithelial cells, iPSC-derived endothelial cells, and iPSC-derived kidney organoids. To date, no human ADPKD iPSC study has addressed the frequent cardiovascular complications and high cardiovascular mortality in ADPKD. Accumulating evidence suggests the causative genes of ADPKD, *PKD1* and *PKD2*, and their derived proteins are associated with cardiac abnormality in animal models. The *PKD2* encoding protein PC2 is a non-specific cation channel and is reported to affect intracellular calcium cycling. The *PKD1* encoding protein PC1 was reported to be involved in L-type calcium channel stability. Because calcium cycling and stability are important to cardiac function and arrhythmia, in our study we used cardiomyocytes derived from ADPKD patient iPSCs to study its primary cellular phenomenon using an electrophysiology approach.

Added value of this study

We efficiently differentiated ADPKD patient iPSCs toward ventricular-like cardiomyocytes and confirmed the PC1 and PC2 expression. Electrophysiological experiments including calcium imaging and whole cell patching were applicable to human iPSC-derived cardiomyocytes. The abnormal calcium cycling and aberrant drug responses of the ADPKD patient iPSC-derived cardiomyocytes were consistent with previous observations in mouse models. More importantly, the close mimicry of the spontaneous beating and drug responsiveness of the patient iPSC-derived cardiomyocytes with the donor patient's clinical phenotypes supported the invaluable role of the iPSC-derived cardiomyocytes to establish an *in vitro*, human cell-based, ADPKD cardiac manifestation model.

Implications of all the available evidence

Deciphering the organ-specific pathophysiology of a human disease with multiple organ involvement is very challenging but is the foundation of novel therapy development. Patient iPSCs carrying a specific mutation are invaluable experimental material enabling us to study a mutated gene causing a phenotype from an organ-specific, tissue-specific, and cell-specific perspective. Our study revealed the close mimicry of iPSC-derived cardiomyocytes with the donor patient's clinical course. The primary cardiac electrophysiological manifestation of ADPKD patient iPSC-derived cardiomyocytes showed the PKD mutation *per se* is a cause of cardiomyocyte calcium cycling abnormality and is proarrhythomgenic. These results pave the way for us to further investigate and evaluate cardiovascular phenotypes in the ADPKD population. In the era of next genetic sequencing, big data, and inter-organ system interaction, establishing a reliable, clinically-relevant, fundamental tool such as patient iPSC-based cellular models, to study organ-, tissue-, and cell type-specific pathogenesis is a crucial complementary validation for developing novel and efficient therapies.

valvular abnormalities, intracranial aneurysm, and aortic dissection/aneurysm [7]. The extent to which these cardiovascular complications are secondary to the progressive renal disease or due to primary manifestations of the mutant protein remains unknown.

ADPKD is attributable to mutations at two gene loci, *PKD1* (16p13.3, 85% of cases) and *PKD2* (4q22, 15% of cases) [8]. Polycystin1 (PC1) and polycystin2 (PC2), encoded by *PKD1* and by *PKD2*, respectively, are expressed in endothelial cells, vascular smooth muscle cells, and cardiomyocytes (CMs) providing potential direct mechanisms for the cardiovascular manifestations of ADPKD [9,10]. Recent evidence indicates that PC1 and PC2 modulate calcium (Ca) cycling and the functional properties of CMs. A decrease in PC1 contributed to pressure overload-induced cardiac hypertrophy in a mouse model through modifying stabilization of the α1C protein of the L-type Ca channel [10]. The heart of mice with *Pkd1*-deficiency showed increased CM apoptosis, fibrosis, and impaired systolic and diastolic function [11]. Decreased PC2 expression altered the Ca transient, shifted the β-adrenergic pathway balance, and cardiac dysfunction [12,13]. Epidemiological analysis showed *PKD2* mutation correlated with idiopathic dilated cardiomyopathy [14]. According to these results, we hypothesized that the cardiac manifestations of ADPKD patients are mutation gene-related and can be modeled at the cellular level.

Human induced pluripotent stem cells (iPSCs) exhibit self-renewal and pluripotency making them a promising cell source for disease modeling, drug discovery and cell therapy [15–18]. iPSCs have been generated from patients with ADPKD to study the vascular pathology, and endothelial cells differentiated from ADPKD-iPSCs showed altered Ca entry and gene expression compared with non-ADPKD controls [19]. However, the link between the ADPKD gene mutations and cardiac manifestations remains obscure. Particularly, studies have not been performed in human CMs to evaluate the impact of ADPKD gene mutations. In this study, we generated ADPKD patient-specific iPSCs and differentiated them toward CMs to decipher the cellular phenotype focusing on Ca handling and drug responses to provide new insight into the clinical cardiovascular manifestations of ADPKD.

2. Materials and methods

2.1. Cell origins and maintenance of undifferentiated hiPSCs

The ADPKD patient-derived iPSC lines from one *PKD1*-mutation subject (*PKD1* Q533X, the iPSC-PKD1 line) and from one *PKD2*-mutation subject (*PKD2* R803X, the iPSC-PKD2 line) were used in our study [20,21]. Two human iPSC normal lines were used as controls, and one of the normal line was applied in the electrophysiological experiment [18]. All of our iPSC lines were generated and authenticated by the Taiwan Human Disease iPSC Service Consortium. We shifted the iPSCs to a feeder-free culture system on Matrigel-coated plates (Corning, NY, USA) and maintained them in daily Essential 8 medium (Thermo Fisher Scientific, Waltham, MA, USA) exchange. The human embryonic stem cell line, H9 (ESC—H9), obtained from WiCell was used in the qPCR experiment as a reference for human pluripotent stem cells.

2.2. Differentiation of hiPSCs toward cardiomyocytes

We adapted the small molecule induction method for CM differentiation [22–24]. Briefly, the medium was changed to cardiac differentiation medium consisting of RPMI 1640 (Thermo Fisher Scientific, Waltham, MA, USA) and B-27 minus insulin supplement (Thermo Fisher Scientific, Waltham, MA, USA); 6–8 μM CHIR99021 (Tocris Bioscience, Bristol, UK) was added on day 0 and day 1. On day 2, the medium was changed to cardiac differentiation medium. On day 3, the medium was changed to cardiac differentiation medium supplemented with 5 μM IWR-1 (Sigma-Aldrich, St. Louis, MO, USA). On day 5, the medium was changed back to cardiac differentiation medium. On day 7 the medium was changed to cardiac medium consisting of RPMI1640 and B-27 supplement (Thermo Fisher Scientific, Waltham, MA, USA), and every other day until dissociation.

2.3. hiPSC-CM dissociation, storage and plating

hiPSC-CMs were incubated with TrypLE Express (Thermo Fisher Science, Waltham, MA, USA) and 1 mg/mL type IV Collagenase (Thermo Fisher Science, Waltham, MA, USA) for 10 min at 37 °C to dissociate cells. hiPSC-CMs were cryopreserved in 10% DMSO and 90% FBS and stored in liquid nitrogen. For our experiments, hiPSC-CMs were thawed and plated at low density on Matrigel growth factor-reduced coated dishes in cardiac medium consisting of RPMI1640 and B-27 supplement.

2.4. Immunostaining and flow cytometry for the hiPSC-CMs

We applied 1:400 mouse α-Actinin (Sigma-Aldrich, St. Louis, MO, USA) for immunostaining. For flow cytometry, we applied 1:100 mouse Troponin-I (Ab19615, Abcam, Cambridge, UK) for the dissociated iPSC-CMs. (Full method can be found in the Supplementary Material).

2.5. Immunoblotting

Primary antibodies including 1:100 mouse anti-PC1 (Santa Cruz Biotechnology, Dallas, TX, USA), 1:200 rabbit anti-PC2 (Santa Cruz Biotechnology, Dallas, TX, USA), and 1:5000 mouse anti-α-Tubulin (Millipore Merck, Darmstadt, Germany) were used for Western blotting. (Full method can be found in the Supplementary Material).

2.6. Real-time quantitative polymerase chain reaction

In each qPCR reaction, the cDNA equivalent of 20 ng of RNA was used. Amplification of cDNA was monitored on an ABI 7500 real-time PCR system (Applied Biosystems, Foster City, CA, USA) with OmicsGreen qPCR Master Mix (Omics Bio, Taipei, Taiwan). Results were normalized to the expression of *ACTB*. The primer sequences are listed in Table S1. (Full method can be found in the Supplementary Material).

2.7. Calcium imaging experiments

Cells were loaded with 2 μM Fura-2 AM (Thermo Fisher Science, Waltham, MA, USA) in Ca-free Tyrode's solution (in mM: NaCl 135, KCl 5.4, $MgCl_2{\cdot}6H_2O$ 1, $NaH_2PO_4{\cdot}H_2O$ 0.5, HEPES 10 and glucose 1; the pH was adjusted to 7.4 by NaOH) at 37 °C for 20 min. Calcium measurements were made by recording the fluorescence ratio of the cells at 340 and 380 nm at room temporature by MetaFluor Fluorescence Ratio Imaging Software (Molecular Devices, Sunnyvale, CA). We recorded the baseline for 40 s, then the cells were exposed to 10 mM caffeine (Sigma-Aldrich, St. Louis, MO, USA) bolus and a total of 300 s of recording was completed.

2.8. Measurement of L-type Ca current

We used the voltage-clamp mode for recording the current of L-type calcium channel (I_{Ca}). The internal solution contained (in mM): CsCl 110, $MgCl_2$ 1, MgATP 5, EGTA 14, and Hepes 20; pH was adjusted to 7.25 with CsOH and the osmolarity was adjusted to 300 mOsm. The external solution contained (in mM): NaCl 134, CsCl 5, $MgCl_2$ 1, $CaCl_2$ 2, glucose 10 and HEPES 10; pH adjusted to 7.4 with NaOH. The iPSC-CMs were held at −70 mV, and a 100-ms conditioning pulse to −40 mV was applied. I_{Ca} were then elicited by 200-ms depolarizing steps ranging from −40 mV to +40 mV (with 10 mV increment). Current densities (pA) were determined to normalize the maximal current amplitude to cell size (pF). Cell membrane capacitance was determined online using Molecular Devices MultiClamp 700B Amplifier (Scientifica, Uckfield, East Sussex, UK).

2.9. Spontaneous action potential recordings

Action potentials (APs) of spontaneously beating iPSC-CMs were recorded by whole-cell current clamping. The Tyrode's solution contained (in mM): NaCl 140, KCl 5.4, $MgCl_2$ 1, $CaCl_2$ 1.8, glucose 10, and HEPES 10; pH was adjusted to 7.4 with NaOH, and oxygenated with 100% O_2 at 37 °C. The internal solution contained (in mM): KCl 120, $MgCl_2$ 1, MgATP 3, EGTA 10, and Hepes 10; pH was adjusted to 7.2 with KOH and the osmolality was adjusted to 300–305 mOsm. All signals were low-pass filtered at 1 kHz and digitized at 10 kHz using a CED Power 1401–3 interface (Cambridge Electronic Design). Data were collected using Signal software (Cambridge Electronic Design, Cambridge, UK).

2.10. Compound solutions used in drug assays

All drugs used in this study were purchased from Sigma-Aldrich. The drug compound solutions were prepared as 10 mmol/L stocks in DMSO, stored at −20 °C, and were diluted in external Tyrode's solution 30 min before treatment.

2.11. Statistical analysis

Statistical analyses and figures were generated by GraphPad Prism 5 software (GraphPad Software, San Diego, CA, USA). Differences among groups were assessed by using one-way ANOVA and two-way ANOVA where appropriate, followed by Bonfferoni *post hoc* test. Drug dose-response of nifedipine was analyzed by repeated measures one-way ANOVA. The half maximal inhibitory concentration (IC_{50}) of nifedipine-induced APD_{90}, APD_{50}, and APD_{25} shortening were calculated by fitting with Hill function. Correlation of the durations of APD_{90}, APD_{50}, and APD_{25} with the beating rates, respectively, were analyzed by linear regression. All data was expressed as mean ± SD unless stated otherwise. Results were considered statistically significant if the P value was <0.05.

3. Results

3.1. Clinical information about the patients from which the ADPKD iPSC lines were generated

Two ADPKD patient iPSC lines had previously been generated and were well characterized as reported [20,21]. The iPSC-PKD1 carrying *PKD1* Q533X mutation was derived from a male with early onset hypertension, myocardial infarction, and kidney failure, who died from sudden cardiac death. His electrocardiogram (EKG) showed normal sinus rhythm with premature ventricular complexes (Fig. S1A) [20]. The iPSC-PKD2 carrying the *PKD2* R803X mutation represents a mutation hotspot in Taiwanese [21,25]. The female patient from which this line was generated had huge bilateral renal cysts and her EKG showed sinus bradycardia with nonspecific ST-T abnormalities (Fig. S1B).

3.2. Patient iPSCs efficiently differentiated to cardiomyocytes

After cardiac lineage induction [22–24], cell morphological changes and cell beating (a clear functional characteristic of CMs) were observed. Immunoflurescence labeling revealed the characterisitc sarcomeric α-actinin expression pattern in these iPSC-CMs (Fig. 1A). Flow cytometry showed that 95.91% of control iPSC-derived CMs (Control-CMs), 96.11% of iPSC-PKD1-derived CMs (PKD1-CMs), and 95.74% of iPSC-PKD2-derived CMs (PKD2-CMs) were troponin I-positive (Fig. 1B). These results demonstrated the high efficiency of cardiac differentiation and the relative purity of the resulting iPSC-CM population.

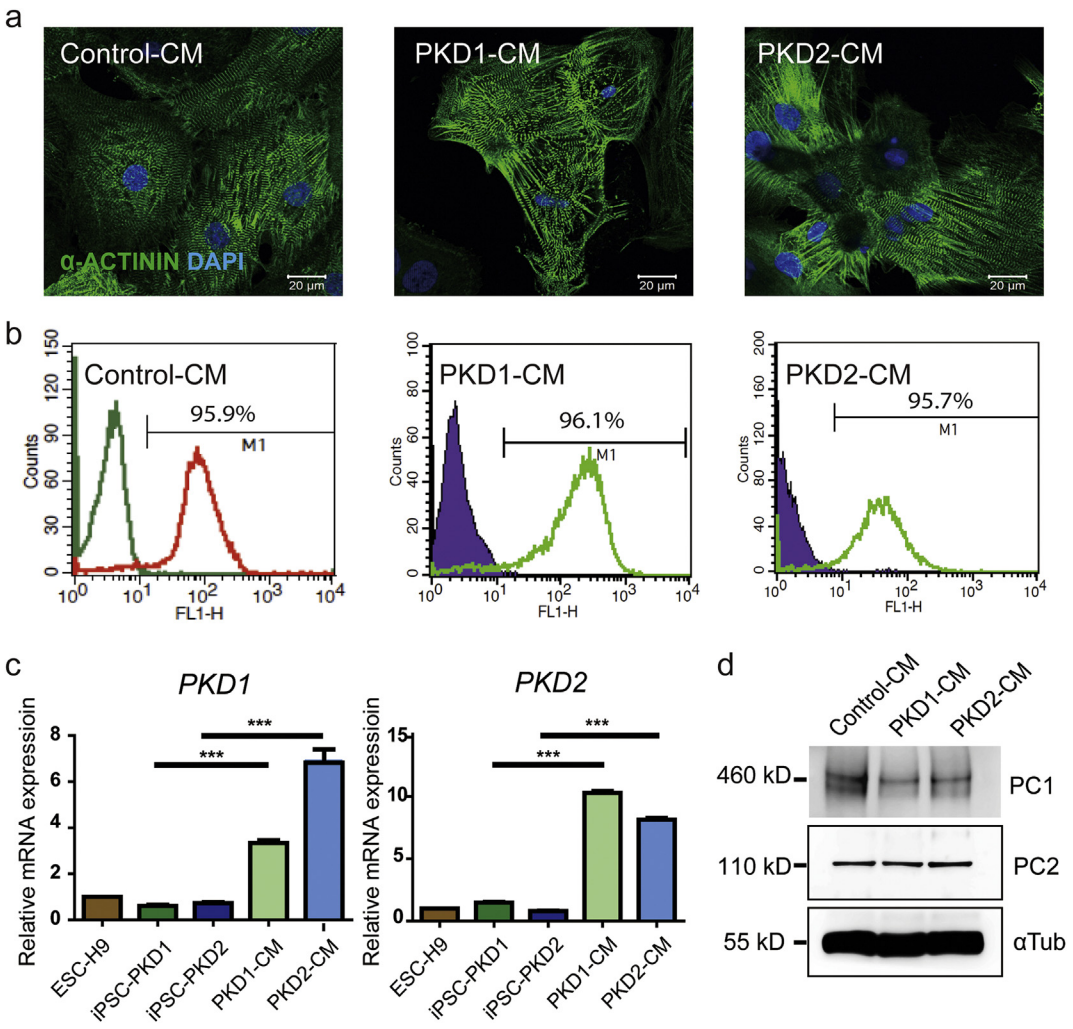

Fig. 1. Cardiomyocytes derived from the ADPKD patient iPSCs had *PKD1* and *PKD2* gene expression, and also PC1 and PC2 protein expression. (A) Immunostaining of α-actinin of the control- and of the patient iPSC-CMs showed the characteristic sarcomeric staining. Scale bar, 20 μm. (B) Percentage of the control- and patient iPSC-CMs exhibiting positive cardiac troponin-I staining. Left peaks represent the isotype control. (C) *PKD1* and *PKD2* gene expression of the ADPKD iPSC-CMs were compared to the undifferentiated iPSCs by quantification PCR. The relative gene expressions were adjusted with the endogenous *ACTB* expression. The bar charts represent the normalized gene expression in ratio to ESC-H9 expression. (D) Western blotting demonstrates the protein expression of polycystin-1 and polycystin-2 in the control- and in patient iPSC-CMs. ESC-H9 represents the human embryonic stem cell line H9; Control-CM, the cardiomyocytes derived from normal subject iPSCs; iPSC-PKD1, the iPSC line carrying the *PKD1* mutation; iPSC-PKD2, the iPSC line carrying the *PKD2* mutation; PC1, polycystine 1; PC2, polycystine 2; and αTub, α-tubulin. Error bars indicated SEM from three independent experiments. ***, $P < 0.001$.

3.3. PKD1 and PKD2 genes and PC1 and PC2 proteins were expressed in iPSC-CMs

PKD1 and *PKD2* gene expression showed significant increase after iPSC lines differentiated to iPSC-CMs by quantitative RT-PCR analysis. (Bar and error bar were generated from three individual experiments, Fig. 1C, Fig. S2). We then checked the PC1 and PC2 protein expression. By Western blotting, lysates from iPSC-CMs revealed doublet bands of PC1 at around 460 kDa, a specific band of PC2 at 110 kDa, and α-tubulin at 55 kDa as the loading control (Fig. 1D, Fig. S2). These results indicated that the iPSC-CMs had *PKD1* and *PKD2* expression at both the gene and the protein levels.

3.4. ADPKD-iPSC-CMs had reduced sarcoplasmic reticulum Ca content and increased L-type Ca current

Given that prior studies using mouse cardiomyocytes suggested changes in intracellular Ca cycling, we used iPSC-CMs after differentiation day 30 loaded with Fura-2-AM to characterize the intracellular Ca cycling [12,22]. The Ca images showed a decreased baseline Ca signal of PKD1-CMs in comparison with Control-CMs, and PKD2-CMs showed no change. Both PKD1-CMs and PKD2-CMs had decreased sarcoplasmic reticulum Ca content in comparison with the Control-CMs as shown by smaller peak and area under the curve after perfusion with 10 mM caffeine (Figs. 2A–C, Control-CM, $n = 118$; PKD1-CM, $n = 79$; PKD2-CM, $n = 61$). The full quantitative data are shown in Table S2.

In cardiomyocytes, L-type Ca currents ($I_{Ca,L}$) play an integral role in triggering Ca cycling and their membrane stability has been suggested to be regulated by PC1 [10]. Next, we performed whole-cell patch clamp studies of quiescent cells at room temperature elicited by stepwise voltage steps to measure the $I_{Ca,L}$ of iPSC-CMs (Fig. 2D). The density of $I_{Ca,L}$ in PKD1-CMs was significantly larger than in Control-CMs at voltages −10 mV, 0 mV, and 10 mV (Fig. 2E); however, there was no significant difference between the control and PKD2-CMs. There was no difference in cell size as assessed by cell capacitance between groups (Fig. 2F). The decreased diastolic Ca level in PKD1-CMs, reduced SR Ca content in PKD1-CMs and PKD2-CMs, with the increased $I_{Ca,L}$ from PKD1-CMs, pointed to clear alterations in Ca cycling in the disease cardiomyocytes that vary between the PKD1 and PKD2 variants. (Figs. 2C and E).

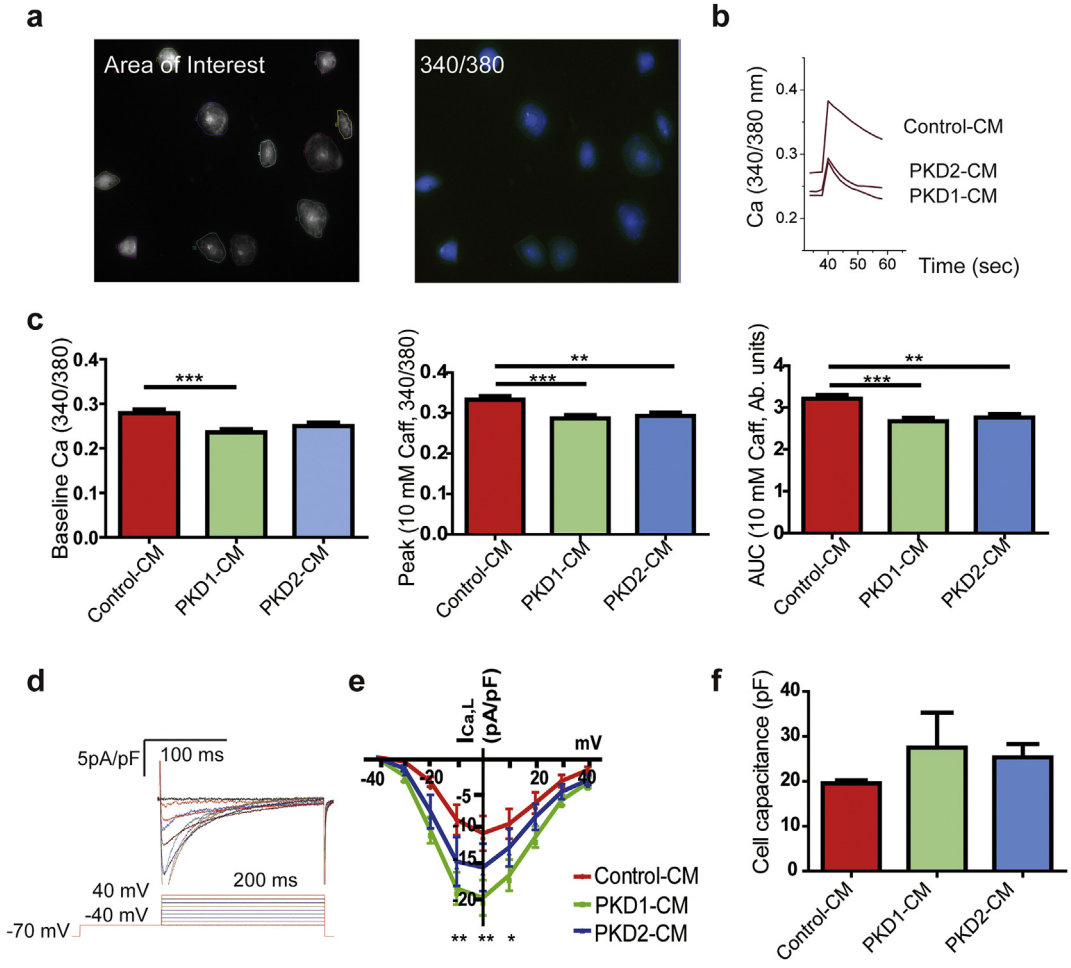

Fig. 2. Calcium handling in cardiomyocytes derived from ADPKD patients' iPSC-CMs. (A) Representative iPSC-CMs loaded with Fura-2 AM showing regions of interest and the 340 nm/380 nm ratio image. (B) Representative calcium transients elicited by the addition of 10 mM caffeine to the iPSC-CMs. (C) Quantification of the baseline calcium, peak, and area under the curve (AUC) of the Ca transient after addition of 10 mM caffeine. Data are the mean ± SEM (Control-CMs, $n = 118$, from four batches of cells generated by two independent differentiation experiments; PKD1-CMs, $n = 79$, from four batches of cells generated by three independent differentiation experiments; PKD2-CMs, $n = 61$, from three batches of cells generated by two independent differentiation experiments.). Error bars indicate SEM. **, $P < 0.01$; ***, $P < 0.001$. (D) Representative example of Ca currents of iPSC-CMs. Voltage protocol is shown below the current record. (E) Current-voltage relationship of peak Ca currents from Control-CMs, PKD1-CMs, and PKD2-CMs. n = 6 cells in each group. Error bars indicate SEM. *, $P < 0.05$; **, $P < 0.01$, PKD1-CM in comparison with Control-CM. (F) Cell membrane capacitances were used to assess cell sizes.

3.5. Baseline action potentials of ADPKD iPSC-CMs

To further examine the electrophysiological properties of the control and the ADPKD patient iPSC-CMs, we next recorded the spontaneous action potentials from single beating cells at 37 °C using whole-cell patch clamp (Fig. 3) [22]. The action potential durations at 90%, 50%, and 25% repolarization (APD_{90}, APD_{50}, and APD_{25}) were calculated. CM phenotypes were defined as ventricular-, nodal-, and atrial-like waveforms by the morphology of the action potentials generated and by the APD_{90}/APD_{50} ratio (Fig. 3A–C). Ventricular-like cells have maximum diastolic potential (MDP) lower than −50 mV, large amplitude (APA) >90 mV, APD_{90}/APD_{50} ratio <1.4, rapid action potential upstroke, and a long plateau phase. Atrial-like cells have MDP lower than −50 mV, APD_{90}/APD_{50} ratio >1.7, and no plateau phase. Nodal-like cells have relatively more positive MDP with an APD_{90}/APD_{50} ratio between 1.4–1.7 [22]. The predominant cell type was ventricular-like cells in all groups, comprising 85% of Control-CMs, 83% of PKD1-CMs, and 89% of PKD2-CMs. The nodal-like cells represented about 10–16% of the iPSC-CMs, while a few cells were classified as atrial-like cells (Fig. 3D).

Quantitative analysis of the spontaneous action potentials showed no differences in MDP, APA, or maximum rate of depolarization (dv/dt_{max}) between groups (Fig. 3E). The PKD2-CM ventricular-like cells had a higher peak voltage of 48 ± 1 mV in comparison with the Control-CMs of 41 ± 1 mV. PKD2-CM ventricular-like cells had longer APD_{90}, APD_{50}, and APD_{25}, respectively, and slower beating rates (Fig. 3E, full numerical data in Table S3). There was a linear correlation between the durations of APD_{90}, APD_{50}, and APD_{25} with the beating rates (Fig. S3). No obvious arrhythmia phenotypes or differences in PKD1-CMs and Control-CMs were observed. But the slower beating rate and longer APD duration of the PKD2-CMs were remarkably similar to the clinical sinus bradycardia phenotype of the specific patient donor of iPSC-PKD2 (Fig. 3E, Fig. S1B).

3.6. Electrophysiological response to L-type Ca channel blocker

Next, we applied whole cell patch clamping of spontaneously beating cells to explore potentially different drug responsiveness between groups. After stable baseline recording for 3 min, we applied serial incremental nifedipine, an L-type Ca channel blocker, solutions for 2 min respectively from 3 nM, 10 nM, 30 nM, 100 nM, and then washout recording under continuous flow of Tyrode's solution (Fig. 4A). The representative long run recordings are shown in Fig. S4A.

The Control-CMs and PKD1-CMs showed nifedipine-induced shortening of phase II repolarization in a dose-dependent manner (Fig. 4B) quantified as dose-dependent decreases in APD_{25}, APD_{50}, and APD_{90} (Fig. 4C). There was no difference in the half maximal inhibitor concentration (IC_{50}) of nifedipine-induced shortening of APD_{90} of the Control-CMs and of the PKD1-CMs (Figs. 4D and S4B). On the other hand, the

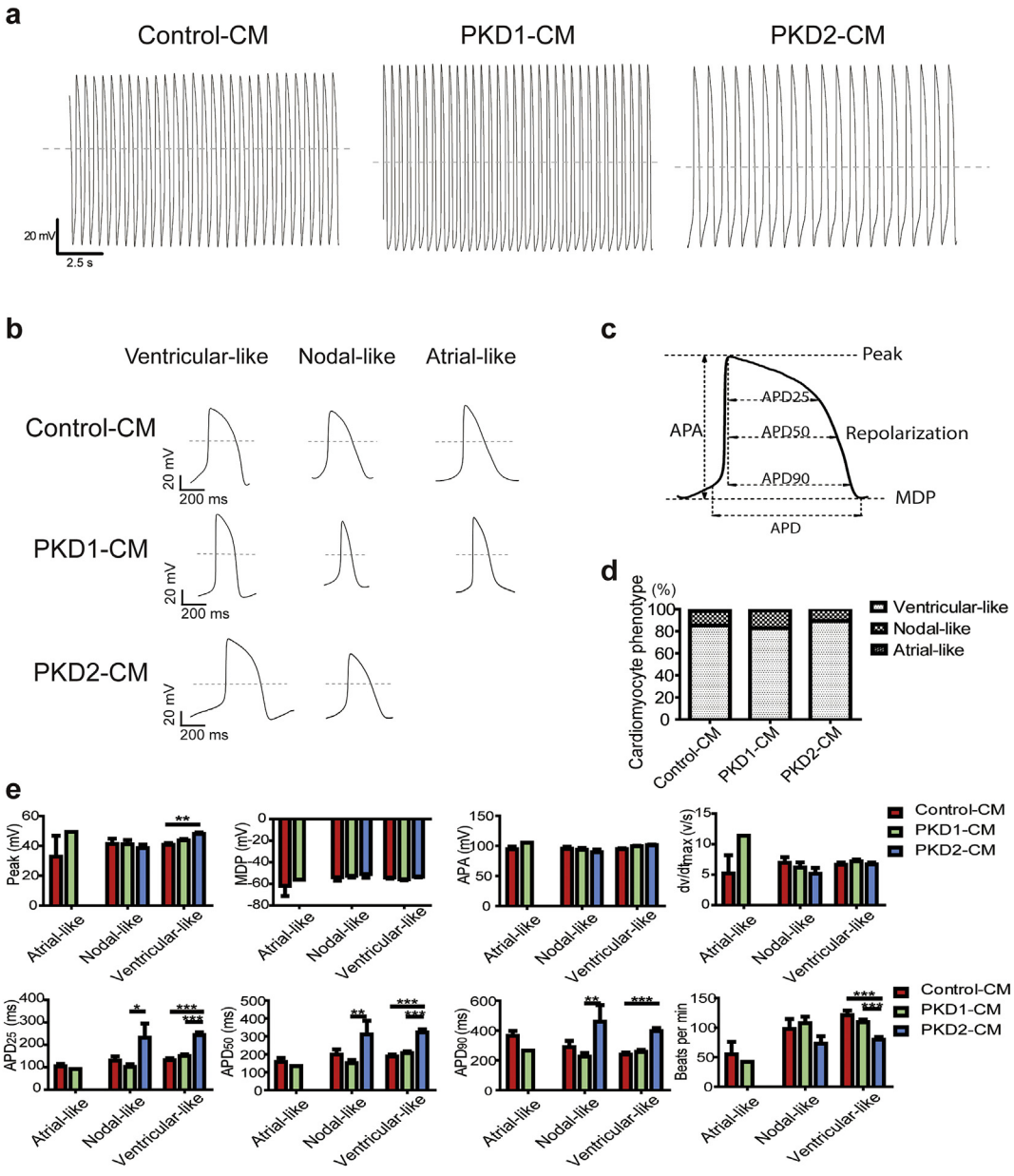

Fig. 3. Baseline action potential characteristics of cardiomyocytes derived from control and ADPKD patient-specific iPSCs. (A) Representative action potential recordings of single beating cells from Control-CM, PKD1-CM, and PKD2-CM using whole-cell patch clamp recording. (B) Representative action potential recordings of ventricular-, nodal-, and atrial-like cells. Dashed lines show 0 mV. (C) Schematic diagram of a patch-clamp trace, demonstrating peak voltage, resting potential as maximum diastolic potential (MDP), amplitude (APA), and action potential duration at 90%, 50%, and 25% repolarization (APD_{90}, APD_{50}, and APD_{25}). (D) Proportions of cardiomyocyte phenotypes of Control-CMs ($n = 130$, from eight batches of cells generated by three independent differentiation experiments), PKD1-CMs ($n = 110$, from seven batches of cells generated by two independent differentiation experiments), and PKD2-CMs ($n = 93$, from six batches of cells generated by two independent differentiation experiments), respectively. (E) Quantitative results from baseline action potential recordings demonstrating peak, MDP, APA, maximum rate of depolarization (dv/dt_{max}), APD_{90}, APD_{50}, APD_{25}, and frequency of cell beating (beats per minute). Error bars indicate SEM. Control-CM, $n = 37$; PKD1-CM, $n = 91$; PKD2-CM, $n = 83$. *, $P < 0.05$, **, $P < 0.01$, ***, $P < 0.001$.

PKD2-CMs showed a relatively blunted response to nifedipine treatment (Fig. 4B, C, and S4B). The full numerical data is presented in Table S4.

By two-way ANOVA, the only significant difference between groups was the slower beating rate in response to nifedipine of PKD2-CMs (Fig. S4C). This information is in line with the baseline slower beating rate of PKD2-CMs (Fig. 3E). We further analyzed the instantaneous beating frequency in response to nifedipine of different groups (Fig. 4E). The PKD1-CMs showed a significant increase in beating rate with nifedipine treatment in comparison with Control-CMs and with PKD2-CMs (Fig. 4F). These data are compatible with the significantly altered Ca baseline, SR Ca content, and the higher $I_{Ca,L}$ density in the baseline recording of PKD1-CMs.

3.7. Electrophysiological response to β-adrenergic agonist

Altered Ca transient but exagerated β-adrenergic response in a $PKD2^{+/-}$ mouse model has been documented leading us to explore the iPSC-CM responsiveness to β-adrenergic stimuli [12]. After baseline recording for 3 min, we applied 1 μM isoproterenol, a non-selective β-adrenergic agonist, for 3 min and then washout with continuous external Tyrode's solution (Fig. 5A). At the cellular level, development of early afterdepolarizations (EADs) and delayed afterdepolarizations (DADs) were considered proarrhythmogenic characteristics [26]. Representative long run recordings are shown in Fig. 5C. Zero out of 15 (0%) Control-CMs, six out of 28 (21.4%) PKD1-CMs, and one out of 20 (5%) PKD2-CMs had baseline DADs. With isoproterenol treatment,

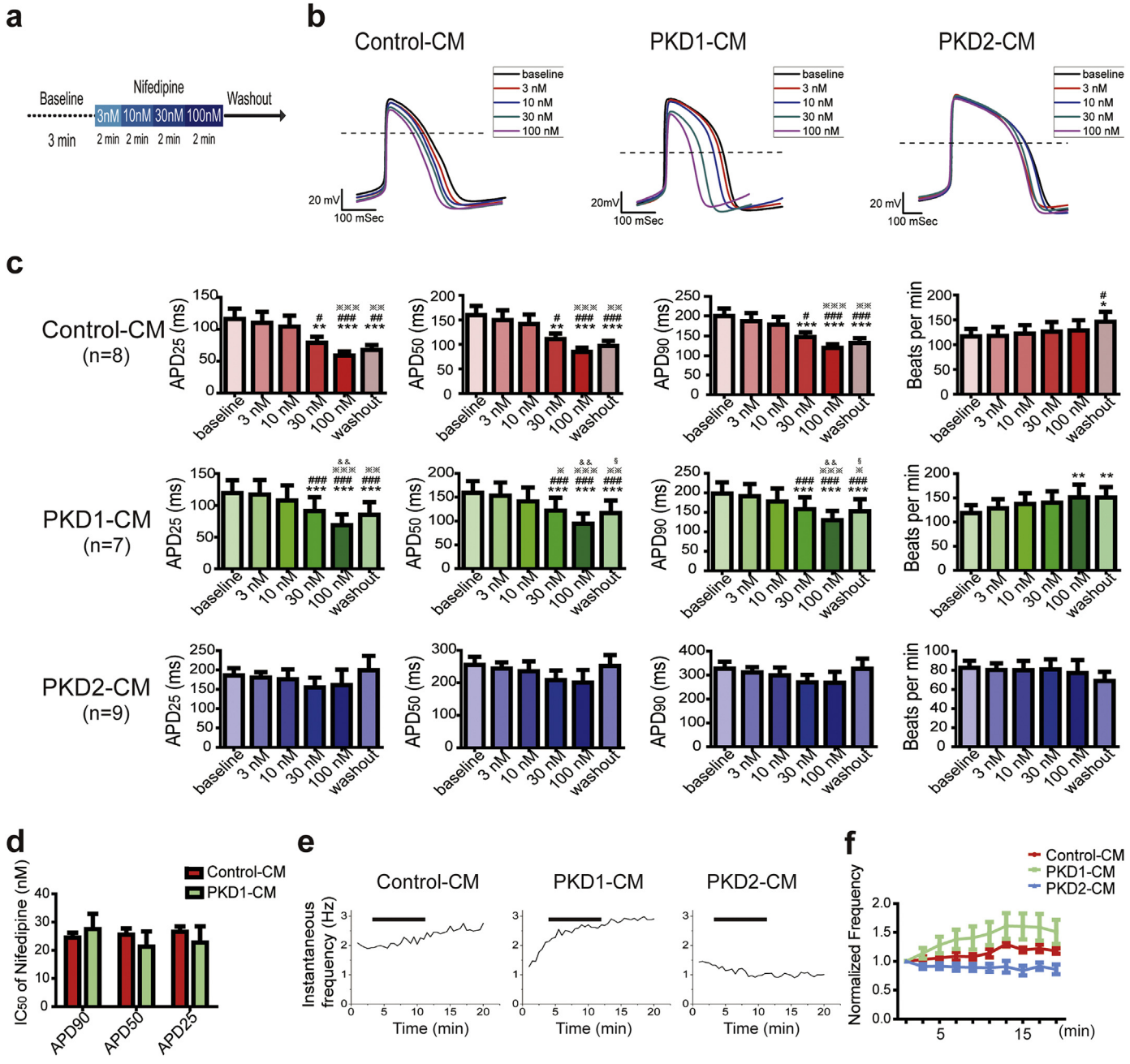

Fig. 4. Comparison of action potential responses to L-type calcium channel blocker, nifedipine, in cardiomyocytes derived from control and ADPKD patient-specific iPSCs. (A) Schematic diagram of the procedure of the nifedipine experiment. With whole cell patching of a single iPSC-CM, a stable baseline recording was obtained for 3 min. And then, escalating doses with nifedipine were sequentially applied for 2 min each. After 100 nM nifedipine treatment for 2 min, the cell was washed with external Tyrode's solution and recorded for 5 more minutes. (B) Representative overlay traces of the effect of nifedipine on Control-CM, PKD1-CM, and PKD2-CM action potentials at doses of 0, 3, 10, 30, and 100 nmol/L (black, red, blue, purple, and magenta traces, respectively). Dashed lines show 0 mV. (C) Analysis of action potential parameters, action potential duration at 90%, 50%, and 25% repolarization (APD_{90}, APD_{50}, and APD_{25}), and beating rates, by repeat measure ANOVA of the Control-CMs, PKD1-CMs, and PKD2-CMs, respectively. Control-CM, n = 8, one batch of cells generated by one differentiation experiment; PKD1-CM, $n = 7$, two batches of cells generated by two differentiation experiments; PKD2-CM, n = 9, two batches of cells generated by one differentiation experiment. *, $P < 0.05$; **, $P < 0.01$; ***, $P < 0.001$, in comparison with baseline; #, $P < 0.05$; ##, $P < 0.01$; ###, $P < 0.001$ in comparison with 3 nM; ※, $P < 0.05$, ※※, $P < 0.01$, ※※※, $P < 0.001$, in comparison with 10 nM; &&, $P < 0.01$, in comparison with 30 nM; §, $P < 0.05$, in comparison with 100 nM. (D) The half maximal inhibitor concentration (IC_{50}) of nifedipine induced APD_{90}, APD_{50}, and APD_{25} shortening of the Control-CMs and PKD1-CM were calculated by fitting with the Hill function. (E) Representative traces of the effects of nifedipine treatment on instantaneous beating frequency of the Control-CM, PKD1-CM, and PKD2-CM, respectively. Black bar represents the nifedipine treatment period. (F) Quantitative analysis of the normalized frequency with nifedipine treatment of the Control-CMs, PKD1-CMs, and PKD2-CMs by two-way ANOVA. Error bars indicate SEM.

four out of 15 (26.7%) Control-CMs, 13 out of 28 (46.4%) PKD1-CMs, and ten out of 20 (50%) PKD2-CMs had isoproterenol elicited DADs (Fig. 5B). These results were in line with the drastic outcome and dysrhythmia clinical phenotype of the specific PKD1 patient. Both PKD1-CM and PKD2-CM shared proarrhythmogenic features elicited by isoproterenol further suggesting a correlation with PKD-associated cardiovascular complications.

4. Discussion

In this study, we provide proof-of-concept that applying patient-specific iPSCs to decipher complicated human diseases such as ADPKD is a feasible approach (Fig. 6). Taking advantage of the efficient iPSC cardiomyocyte differentiation, we first verified the change in Ca handling and drug responsiveness of the ADPKD iPSC-CMs. More

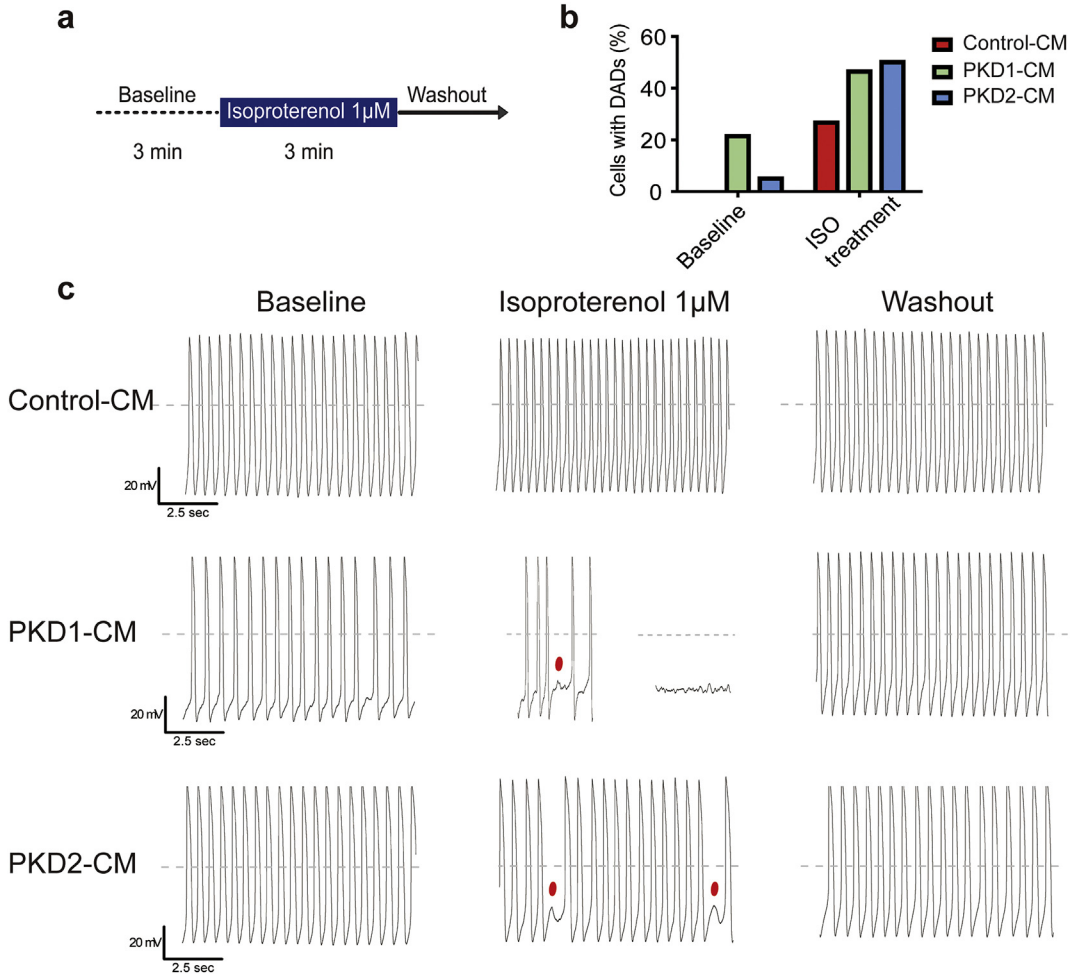

Fig. 5. Action potential (AP) responses to β-adrenergic agonist, isoproterenol, in cardiomyocytes derived from control and ADPKD patient-specific iPSCs. (A) Schematic diagram of the procedure of the isoproterenol experiment. With whole cell patching of a single iPSC-CM, stable baseline recording was obtained for 3 min. Next, 1 μM isoproterenol was applied for 3 min, and then the cell was washed with external Tyrode's solution and recorded for 5 more minutes. (B) Percentage of cells showing delay after depolarization (DAD) at baseline and with isoproterenol treatment. (C) Representative AP tracing of the iPSC-CMs from each group during the isoproterenol experiment, respectively. Dashed lines show 0 mV. Red dots indicate DAD. Control-CMs, $n = 15$, one batch of cells generated from one differentiation experiment; PKD1-CMs, $n = 28$, four batches of cells generated by two differentiation experiments; PKD2-CMs, $n = 20$, four batches of cells generated by two differentiation experiments.

specifically, the slower beating rate, longer APD period, and relatively blunted response to nifedipine treatment of PKD2-CMs clearly recapitulated the clinical phenotype of sinus bradycardia of the donor. The decreased baseline and SR Ca content, larger $I_{Ca,L}$ density, dramatic dose-response and frequency response to nifedipine treatment of PKD1-CMs closely matched the clinical outcome of the donor. Both of these ADPKD iPSC-CMs showed increased DADs after isoproterenol treatment, suggesting common proarrhythmogenic characteristics. These electrophysiological differences at the cellular level of patient iPSC-CMs support the potential role of the disease mutation gene *per se* in contributing to ADPKD-associated cardiovascular complications.

Studies on the proteins PC1 and PC2, encoded by the disease causative genes *PKD1* and *PKD2*, respectively, have identified a bewildering array of signaling pathways and regulatory processes [1,8]. Despite promising results in PKD animal models, clinical trials targeting mechanisms such as the mTOR-pathway, cAMP-pathway, or renin-angiotensin-aldosterone system showed no or only moderate effects [5,6,27]. Animal models were unable to fully recapitulate human responses and these species-specific discrepancies highlight the significance of using human cells for disease modeling and drug development. The advances in human iPSC technologies have enabled scientists to develop novel human cell-based, *in vitro*, disease models [15]. A pioneer study by Freedman showed that *PKD1*-mutant patient iPSC-derived epithelial cells have decreased PC2 expression in cilia [28]. *PKD* mutant human iPSC-derived kidney organoids showed promising results in modeling ADPKD cystogenesis [29,30]. To the best of our knowledge, this is the first report to apply iPSC-derived CMs to the study of ADPKD cardiac electric characterization for modeling ADPKD extra-renal manifestations. As yet, no clear correlation between severity of disease phenotype and the position of the mutation for ADPKD have been reported [31–34]. We used the *PKD1* mutation line iPSC-PKD1 carrying Q533X mutation which has a strong family history of cardiovascular complication, and the *PKD2* mutation line iPSC-PKD2 carrying R803X at *PKD2*, which represents the hot mutation spot in Taiwan, in our study [20,21,25].

Using the small molecule induction method, the iPSC-CMs we generated were of high purity and ventricular-like cells were predominant [22–24]. The iPSC-CMs had *PKD1* and *PKD2* expression at both the gene and the protein level. PC2 has a molecular weight of ~110 kDa and the doublet bands of PC1 are considered the N-terminal fragment subunits of PC1 after autoproteolysis at the G protein-coupled receptor proteolytic site [35]. The decreased SR Ca content and the increased $I_{Ca,L}$ density of PKD1-CMs suggests a compensatory mechanism [36]. PC1 encoded by *PKD1*, is a transmembrane protein with a multidomain structure, a large extracellular N-terminal, and an intracellular C-terminal. The mutation of iPSC-PKD1 was *PKD1* Q533X, which is located next to the C-type lectin domain (403–532) at the extracellular

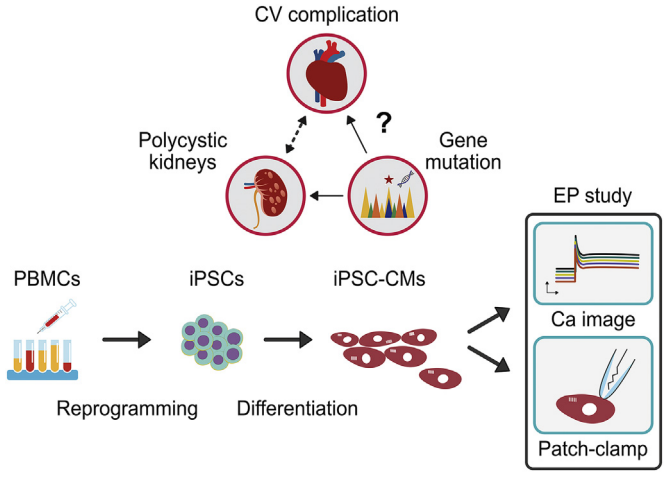

Fig. 6. Schematic diagram modeling ADPKD cardiac electrical characterization with patient iPSC-CMs. The direct link between gene mutations in ADPKD patients and the high occurrence of cardiovascular complications is obscure. We generated ADPKD patient-specific iPSCs by reprogramming their peripheral blood mononuclear cells. The ADPKD patient-specific iPSCs were then differentiated toward cardiomyocytes (CMs). By applying calcium image study and whole cell patch clamping, we explored the electrophysiological properties and correlated them with the clinical cardiovascular phenotypes. CV, cardiovascular; PBMCs, peripheral blood mononuclear cells; iPSCs, induced pluripotent stem cells; iPSC-CMs, cardiomyocytes-derived from iPSCs; EP, electrophysiology; Ca, Calcium.

N-terminal of PC1. The C-type lectin domain of PC1 is predicted to function in Ca-dependent carbohydrate binding [37,38]. A mouse stretch-induced cardiac hypertrophy model study reported that PC1 effected the stability of the L-type Ca channel [10]. In addition, PKD2-CMs also had decreased SR Ca content. Therefore, our data from human iPSC-CMs are in line with the earlier reports from animal models suggesting PC1 or PC2 haploinsufficiency disrupts intracellular Ca homeostasis. These results echoed the recent treatment of ADPKD targeting the cAMP signaling pathway and vasopressin receptor in kidney cells [27]. Tolvaptan, a vasopressin receptor 2 antagonist, is the present treatment of choice for ADPKD [6]. With the bewildering array of PC1 and PC2 associated signal pathways and protein-protein interactions, the therapeutic effect of Tolvaptan highlights the important role of PC1 and PC2 induced disruption of intracellular calcium homeostasis in the pathogenesis of ADPKD. Evidence suggests the reduced level of functional PC1 or PC2 directly induced reduction in intracellular calcium and indirectly dysregulated cAMP metabolism and the purinergic signaling pathway [27]. Whether this linkage could be generalized in cardiomyocytes and causes the cardiovascular complication of ADPKD will need further investigation.

We further examined the spontaneously beating cells for their baseline action potentials and their responses to nifedipine, an L-type Ca channel blocker. The Contol-CMs and PKD1-CMs showed dose-dependent shortening of phase II repolarization in response to nifedipine treatment. The slower spontaneous beating rate at baseline and blunted responses to nifedipine treatment characterized the electric phenotype of PKD2-CMs. This closely mimicked the clinical sinus bradycardia of this specific patient. The iPSC-PKD2 line carried the *PKD2* R803X mutation, which is located in the C-terminal of PC2. PC2 encoded by *PKD2* is a 968 amino acid transmembrane protein with intracellular N- and C-terminals [8]. PC2 functions as a Ca-permeable nonselective cation channel and is a member of the transient receptor potential family, TRPP2 [8]. In CMs, PC2 was reported to interact with and regulate ryanodine receptor 2 by acting as a brake for Ca release of SR [12]. Mutation of iPSC-PKD2, *PKD2* R803X, is located near the S812 phosphorylation site for sequestering PC2 at ER/SR [39]. However, how this mutation gene affects the autonomous cardiac cycling will need further investigation. In our study, the small number (n) of atrial and nodal cells predisposed the results to large standard deviation and statistical insignificance. Therefore, there is a limitation in our study regarding the ventricular-like cell predominance. Another differentiation protocol to generate more atrial-like or nodal-like cells from human iPSCs will be needed to further investigate the cardiac automaticity.

Clinically, the heart rate in patients is regulated by multiple features including the autonomic nervous system. We would like to focus on clinical correlations to other arrhythmic behavior. Most cardiovascular deaths result from heart failure, coronary artery disease, or arrhythmia-related sudden cardiac death [4,7]. The *Pkd*-deficient animal model suggested altered Ca handling affected the β-adrenergic response of CMs [12]. We therefore tested isoproterenol, a non-specific β-adrenergic agonist, on the proarrhythmogenic response of iPSC-CMs. DAD has been suggested to come from the I_{NCX}, current of the sodium/Ca exchange channel, and resulted in arrhythmia in cardiac rhythm [26,40]. In our results, PKD1-CMs showed the most unstable baseline recording with DADs and two times more DADs in response to isoproterenol in comparison with Control-CMs. This proarrhythmogenic character at the cellular level was obviously comparable with the patient's clinical ventricular premature beats and sudden cardiac death (Fig 5B, C, and S1). In addition, PKD2-CMs also expressed more DADs after isoproterenol treatment, which suggest a common phenomenon of *PKD* gene mutation linked to the cardiovascular morbidity and mortality of ADPKD. Although cardiac arrhythmias are not commonly associated with ADPKD, the presence of cardiac hypertrophy clearly increases the risk of arrhythmias. Furthermore, it is possible that a second 'hit' along with the *PKD* gene mutation may increase the risk of arrhythmias. Further study will be needed to comprehensively evaluate the genetic background and to decipher the mechanisms of the mutation genes leading to ADPKD cardiovascular complications.

In this study, our primary object was proof-of-concept of application of iPSC-CMs for studying a complex human disease. We report the first study examining the primary electrophysiological manifestation of ADPKD patient iPSC-CMs. Our data reveal the mutated gene related to the cardiovascular complication of ADPKD. These findings support further work to explicate the mechanism in the future, including how the mutated genes contribute to the cardiovascular complication. We agree that the big challenge with stem cell experiments is the relative heterogeneity from line to line and even from clone to clone. The genetic heterogeneity of iPSCs is well-characterized and is mostly attributed to donor factors [41]. The variations may also be induced or selected by the reprogramming process, or accumulated in culturing [42]. Therefore, monitoring and validating the genetic background of the iPSC lines is important in the application of stem cell science. Nevertheless, the precisely recapitulated phenotype of iPSCs at the cellular level supported its valuable role in studying complex human disease [43]. Since large-scale stem cell experiments are difficult, costly, and could still not fully eliminate these concerns, one feasible approach would be the emerging new tool of gene editing [44,45]. The cellular phenotype of a disease line in comparison with its precise gene corrected isogenic control would be more powerful to strengthen the findings of stem cell research. Although our present results come from two disease lines in comparison with normal lines, findings for both PKD1 and PKD2 share features that are consistent with similar pathophysiology in the clinic, supporting the biological robustness of our results.

In summary, we demonstrated successful ventricular cell predominant cardiomyocyte differentiation from human iPSCs. The electrophysiological parameters including the Ca images, Ca currents, and spontaneous action potentials of the ADPKD patient-specific iPSC-CMs exhibited a cellular phenotype that was closely correlated with the clinical phenotype of the specific patients. We have therefore displayed a new approach to decipher kidney disease with multiple organ involvement by using patient-specific iPSCs. ADPKD is a systemic disorder with many extra-renal manifestations, our study supports the notion that the role of the mutation gene *per se* might contribute to its cardiovascular complication. Larger scale and more comprehensive evaluation will be needed to address the ADPKD patient's cardiovascular presentation and to develop novel therapies.

Acknowledgements

We thank Dr. Ling-Hui Li for consultation. We thank the Taiwan Human Disease iPSC Service Consortium for iPSC generation and technical support.

Funding sources

This work was supported by the Ministry of Science and Technology, Taiwan (MOST 106-2811-B-001-036 and 106-2319-B-001-003), the National Health Research Institutes grant EX106-10512SI, and the Academia Sinica Program for Technology Supporting Platform Axis (TSPA) Scheme, Thematic Research Program and Summit Research Program. The mutation gene analysis and clinical evaluations were supported by grant MOST104–2314-B-037-066 (to D.Y.H.) and grant MOST107–2314-B-037-019-MY3, KMUH103-3 M06, KMUH104-4 M10 (to J.J.L.).

Conflicts of interest

None.

Author contributions

H.C.C. and P.C.H. conceived the strategy and supervised the project; J.J.L. designed the study; J.J.L., S.J.C., C.Y.H., C.Y.C., F.L., and D.Y.H. carried out experiments; J.J.L. and S.J.C. analyzed the results and made the figures; J.J.L. drafted the paper; T.J.K., H.C.C. and P.C.H. critically revised the paper; all authors approved the final version of the manuscript.

Appendix A. Supplementary data

Supplementary data to this article can be found online at https://doi.org/10.1016/j.ebiom.2019.01.011.

References

[1] Torres VE, Harris PC, Pirson Y. Autosomal dominant polycystic kidney disease. Lancet 2007;369:1287–301.
[2] Luciano RL, Dah NK. Extra-renal manifestations of autosomal dominant polycystic kidney disease (ADPKD): considerations for routine screening and management. Nephrol Dial Transplant 2014;29:247–54.
[3] Fick GM, Johnson AM, Hammond WS, Gabow PA. Causes of death in autosomal dominant polycystic kidney disease. J Am Soc Nephrol 1995;5:2048–56.
[4] Perrone RD, Ruthazer R, Terrin NC. Survival after end-stage renal disease in autosomal dominant polycystic kidney disease: contribution of extrarenal complications to mortality. Am J Kidney Dis 2001;38:777–84.
[5] Ong AC, Devuyst O, Knebelmann B, Walz G. ERA-EDTA Working Group for Inherited Kidney Diseases: Autosomal dominant polycystic kidney disease: the changing face of clinical management. Lancet 2015;385:1993–2002.
[6] Torres VE, Chapman AB, Devuyst O, Gansevoort RT, Perrone RD, Koch G, et al. Tolvaptan in later-stage autosomal dominant polycystic kidney disease. N Engl J Med 2017;377:1930–42.
[7] Ecder T, Schrier RW. Cardiovascular abnormalities in autosomal-dominant polycystic kidney disease. Nat Rev Nephrol 2009;5:221–8.
[8] Chapin HC, Caplan MJ. The cell biology of polycystic kidney disease. J Cell Biol 2010;191:701–10.
[9] Volk T, Schwoerer AP, Thiessen S, Schultz JH, Ehmke H. A polycystin-2-like large conductance cation channel in rat left ventricular myocytes. Cardiovasc Res 2003;58:76–88.
[10] Pedrozo Z, Criollo A, Battiprolu PK, Morales CR, Contreras-Ferrat A, Fernández C, et al. Polycystin-1 is a cardiomyocyte mechanosensor that governs L-Type Ca2+ channel protein stability. Circulation 2015;131:2131–42.
[11] Balbo BE, Amaral AG, Fonseca JM, de Castro I, Salemi VM, Souza LE, et al. Cardiac dysfunction in Pkd1-deficient mice with phenotype rescue by galectin-3 knockout. Kidney Int 2016;90:580–97.
[12] Kuo IY, Kwaczala AT, Nguyen L, Russell KS, Campbell SG, Ehrlich BE. Decreased polycystin 2 expression alters calcium-contraction coupling and changes β-adrenergic signaling pathways. Proc Natl Acad Sci U S A 2014;111:16604–9.
[13] Kuo IY, Duong SL, Nguyen L, Ehrlich BE. Decreased polycystin 2 levels result in non-renal cardiac dysfunction with aging. PLoS One 2016;11:e0153632.
[14] Paavola J, Schliffke S, Rossetti S, Kuo IY, Yuan S, Sun Z, et al. Polycystin-2 mutations lead to impaired calcium cycling in the heart and predispose to dilated cardiomyopathy. J Mol Cell Cardiol 2013;58:199–208.
[15] Takahashi K, Tanabe K, Ohnuki M, Narita M, Ichisaka T, Tomoda K, et al. Induction of pluripotent stem cells from adult human fibroblasts by defined factors. Cell 2007;131:861–72.
[16] Fox IJ, Daley GQ, Goldman SA, Huard J, Kamp TJ, Trucco M. Stem cell therapy. Use of differentiated pluripotent stem cells as replacement therapy for treating disease. Science 2014;345:1247391.
[17] Benedetti V, Brizi V, Guida P, Tomasoni S, Ciampi O, Angeli E, et al. Engineered kidney tubules for modeling patient-specific diseases and drug discovery. EBioMedicine 2018;33:253–68.
[18] Hsu WT, Huang CY, Yen CYT, Cheng AL, Hsieh PCH. The HER2 inhibitor lapatinib potentiates doxorubicin-induced cardiotoxicity through iNOS signaling. Theranostics 2018;8:3176–88.
[19] Ameku T, Taura D, Sone M, Numata T, Nakamura M, Shiota F, et al. Identification of MMP1 as a novel risk factor for intracranial aneurysms in ADPKD using iPSC models. Sci Rep 2016;6:30013.
[20] Lee JJ, Ho MC, Huang CY, Wen CH, Cheng YC, Hsu YH, et al. Induced pluripotent stem cells derived from an autosomal dominant polycystic kidney disease patient carrying a PKD1 Q533X mutation. Stem Cell Res 2017;25:83–7.
[21] Ho MC, Huang CY, Lee JJ, Hsu SH, Cheng YC, Hsu YH, et al. Generation of an induced pluripotent stem cell line, IBMS-iPSC-014-05, from a female autosomal dominant polycystic kidney disease patient carrying a common mutation of R803X in PKD2. Stem Cell Res 2017;25:38–41.
[22] Burridge PW, Matsa E, Shukla P, Lin ZC, Churko JM, Ebert AD, et al. Chemically defined generation of human cardiomyocytes. Nat Methods 2014;11:855–60.
[23] Lian X, Hsiao C, Wilson G, Zhu K, Hazeltine LB, Azarin SM, et al. Robust cardiomyocyte differentiation from human pluripotent stem cells via temporal modulation of canonical Wnt signaling. Proc Natl Acad Sci U S A 2012;109:E1848–57.
[24] Hwang HS, Kryshtal DO, Feaster TK, Sánchez-Freire V, Zhang J, Kamp TJ, et al. Comparable calcium handling of human iPSC-derived cardiomyocytes generated by multiple laboratories. J Mol Cell Cardiol 2015;85:79–88.
[25] Chang MY, Chen HM, Jenq CC, Lee SY, Chen YM, Tian YC, et al. Novel PKD1 and PKD2 mutations in Taiwanese patients with autosomal dominant polycystic kidney disease. J Hum Genet 2013;8:720–7.
[26] Liang P, Lan F, Lee AS, Gong T, Sanchez-Freire V, Wang Y, et al. Drug screening using a library of human induced pluripotent stem cell-derived cardiomyocytes reveals disease-specific patterns of cardiotoxicity. Circulation 2013;127:1677–91.
[27] Chebib FT, Sussman CR, Wang X, Harris PC, Torres VE. Vasopressin and disruption of calcium signalling in polycystic kidney disease. Nat Rev Nephrol 2015;11:451–64.
[28] Freedman BS, Lam AQ, Sundsbak JL, Iatrino R, Su X, Koon SJ, et al. Reduced ciliary polycystin-2 in induced pluripotent stem cells from polycystic kidney disease patients with PKD1 mutations. J Am Soc Nephrol 2013;24:1571–86.
[29] Freedman BS, Brooks CR, Lam AQ, Fu H, Morizane R, Agrawal V, et al. Modelling kidney disease with CRISPR-mutant kidney organoids derived from human pluripotent epiblast spheroids. Nat Commun 2015;6:8715.
[30] Cruz NM, Song X, Czerniecki SM, Gulieva RE, Churchill AJ, Kim YK, et al. Organoid cystogenesis reveals a critical role of microenvironment in human polycystic kidney disease. Nat Mater 2017;16:1112–9.
[31] Rossetti S, Hopp K, Sikkink RA, Sundsbak JL, Lee YK, Kubly V, et al. Identification of gene mutations in autosomal dominant polycystic kidney disease through targeted resequencing. J Am Soc Nephrol 2012;23:915–33.
[32] Igarashi P, Somlo S. Genetics and pathogenesis of polycystic kidney disease. J Am Soc Nephrol 2002;13:2384–98.
[33] Tan YC, Blumenfeld J, Rennert H. Autosomal dominant polycystic kidney disease: genetics, mutations and microRNAs. Biochim Biophys Acta 2011;1812:1202–12.
[34] Woon C, Bielinski-Bradbury A, O'Reilly K, Robinson P. A systematic review of the predictors of disease progression in patients with autosomal dominant polycystic kidney disease. BMC Nephrol 2015;16:140.
[35] Kurbegovic A, Kim H, Xu H, Yu S, Cruanès J, Maser RL, et al. Novel functional complexity of polycystin-1 by GPS cleavage in vivo: role in polycystic kidney disease. Mol Cell Biol 2014;34:3341–53.
[36] Koivumäki JT, Takalo J, Korhonen T, Tavi P, Weckström M. Modelling sarcoplasmic reticulum calcium ATPase and its regulation in cardiac myocytes. Philos Trans A Math Phys Eng Sci 2009;367:2181–202.
[37] The International Polycystic Kidney Disease Consortium. Polycystic kidney disease: the complete structure of the PKD1 gene and its protein. Cell 1995;81:289–98.
[38] Weston BS, Malhas AN, Price RG. Structure-function relationships of the extracellular domain of the autosomal dominant polycystic kidney disease-associated protein, polycystin-1. FEBS Lett 2003;538:8–13.
[39] Tsiokas L, Kim S, Ong EC. Cell biology of polycystin-2. Cell Signal 2007;19:444–53.
[40] Hoekstra M, Mummery CL, Wilde AA, Bezzina CR, Verkerk AO. Induced pluripotent stem cell derived cardiomyocytes as models for cardiac arrhythmias. Front Physiol 2012;3:346.
[41] Kilpinen H, Goncalves A, Leha A, Afzal V, Alasoo K, Ashford S, et al. Common genetic variation drives molecular heterogeneity in human iPSCs. Nature 2017;546:370–5.
[42] Liang G, Zhang Y. Genetic and epigenetic variations in iPSCs: potential causes and implications for application. Cell Stem Cell 2013;13:149–59.
[43] Warren CR, O'Sullivan JF, Friesen M, Becker CE, Zhang X, Liu P, et al. Induced pluripotent stem cell differentiation enables functional validation of GWAS variants in metabolic disease. Cell Stem Cell 2017;20:547–57.
[44] Hsu PD, Lander ES, Zhang F. Development and applications of CRISPR-Cas9 for genome engineering. Cell 2014;157:1262–78.
[45] Firth AL, Menon T, Parker GS, Qualls SJ, Lewis BM, Ke E, et al. Functional gene correction for cystic fibrosis in lung epithelial cells generated from patient iPSCs. Cell Rep 2015;12:1385–90.